Contents lists available at ScienceDirect

NeuroImage: Clinical

Longitudinal brain atrophy and CSF biomarkers in early-onset Alzheimer's disease

José Contador [a], Agnès Pérez-Millán [a], Adrià Tort-Merino [a], Mircea Balasa [a,b], Neus Falgàs [a,b,c], Jaume Olives [a], Magdalena Castellví [a], Sergi Borrego-Écija [a], Beatriz Bosch [a], Guadalupe Fernández-Villullas [a], Oscar Ramos-Campoy [a], Anna Antonell [a], Nuria Bargalló [d], Raquel Sanchez-Valle [a,e], Roser Sala-Llonch [f,g,1], Albert Lladó [a,e,1,*], for the Alzheimer's Disease Neuroimaging Initiative[2]

[a] Alzheimer's Disease and Other Cognitive Disorders Unit, Neurology Service, Hospital Clínic of Barcelona, Institut d'Investigacions Biomèdiques August Pi i Sunyer (IDIBAPS), Universitat de Barcelona, Barcelona 08036, Spain
[b] Atlantic Fellow for Equity in Brain Health, Global Brain Heath Institute
[c] Department of Neurology, Memory & Aging Center, Weill Institute for Neurosciences, University of California, 675 Nelson Rising Lane, Suite 190, San Francisco, CA 94158, USA
[d] Image Diagnostic Centre, IDIBAPS, Hospital Clínic de Barcelona, Barcelona, Spain
[e] Centro de Investigación Biomédica en Red de Enfermedades Neurodegenerativas. CIBERNED, Spain
[f] Institute of Neurosciences. Department of Biomedicine, Faculty of Medicine, University of Barcelona, Barcelona, 08036, Spain
[g] Biomedical Imaging Group, Biomedical Research Networking Center in Bioengineering, Biomaterials and Nanomedicine (CIBER-BBN), Barcelona, Spain

ARTICLE INFO

ABSTRACT

There is evidence of longitudinal atrophy in posterior brain areas in early-onset Alzheimer's disease (EOAD; aged < 65 years), but no studies have been conducted in an EOAD cohort with fluid biomarkers characterization. We used 3T-MRI and Freesurfer 6.0 to investigate cortical and subcortical gray matter loss at two years in 12 EOAD patients (A + T + N +) compared to 19 controls (A-T-N-) from the Hospital Clínic Barcelona cohort. We explored group differences in atrophy patterns and we correlated atrophy and baseline CSF-biomarkers levels in EOAD. We replicated the correlation analyses in 14 EOAD (A + T + N +) and 55 late-onset AD (LOAD; aged ≥ 75 years; A + T + N +) participants from the Alzheimer's disease Neuroimaging Initiative. We found that EOAD longitudinal atrophy spread with a posterior-to-anterior gradient and beyond hippocampus/amygdala. In EOAD, higher initial CSF NfL levels correlated with higher ventricular volumes at baseline. On the other hand, higher initial CSF Aβ42 levels (within pathological range) predicted higher rates of cortical loss in EOAD. In EOAD and LOAD subjects, higher CSF t-tau values at baseline predicted higher rates of subcortical atrophy. CSF p-tau did not show any significant correlation. In conclusion, posterior cortices, hippocampus and amygdala capture EOAD atrophy from early stages. CSF Aβ42 might predict cortical thinning and t-tau/NfL subcortical atrophy.

---

1. Introduction

According to the arbitrary cut-off age of 65 years, Alzheimer's disease (AD) is classified as early-onset AD (EOAD, aged < 65 years) or late-onset AD (LOAD, aged > 65 years). Both variants share the same pathological landmarks, such as underlying amyloid plaques, neurofibrillary tangles (NFT) and progressive neurodegeneration. However, early-onset presentations might constitute a distinct and more severe variant of AD (Mendez, 2012) in which AD-pathology distributes differently. While the limbic areas are predominantly affected in LOAD, EOAD patients show a higher burden of NFT in neocortical regions (Marshall et al., 2007; Murray et al., 2011).

These neuropathological features go along with higher rates of non-amnestic symptoms (Koedam et al., 2010) and faster cognitive decline in EOAD (Wattmo and Wallin, 2017). On the other hand, cross-sectional studies using magnetic resonance imaging (MRI) reveal a pattern of widespread atrophy in EOAD particularly marked in parietal areas, whereas in LOAD, atrophy is restricted to temporal regions (Aziz et al., 2017; Harper et al., 2017; Möller et al., 2013; Ossenkoppele et al., 2015a). Longitudinal MRI studies suggest that, in EOAD, the associative cortices are more vulnerable to atrophy than the medial temporal lobe (MTL), and that the atrophy rates are faster than those in LOAD (Cho et al., 2013a; Fiford et al., 2018; Joie et al., 2020; Migliaccio et al., 2015). However, the conclusions drawn by prior studies regarding a specific pattern of longitudinal atrophy for EOAD are not clear as many of them include subjects in whom the clinical diagnosis of AD was not supported by the use of biomarkers or who were not obtained from specific EOAD cohorts.

In 2018, the National Institute on Aging-Alzheimer's Association (NIA-AA) Research Framework redefined the AD continuum in terms of three groups of biomarkers: amyloid (A), tau (T) and neurodegeneration (N) (Jack et al., 2018), namely the ATN profile. The ATN profile can be evaluated through neuroimaging or biofluids (e.g. cerebrospinal fluid (CSF)). In this context, longitudinal patterns of progressive atrophy could help to identify regions of early neurodegeneration in EOAD, in whom the MTL seems to not optimally reflect the spread of the disease (Falgàs et al., 2019; Murray et al., 2011).

There is a poor understanding of how longitudinal changes in MRI interact with other biomarkers, especially in EOAD. Similar to LOAD patients, the presence of low levels of CSF amyloid-β1-42 (Aβ42) with high levels of phosphorylated Tau (p-tau) and total Tau (t-tau) define the diagnosis in EOAD (Jack et al., 2018; McKhann et al., 2011). Some studies have suggested that baseline CSF Tau and neurofilament light chain (NfL) levels could predict longitudinal atrophy in AD (Fjell et al., 2010; Tarawneh et al., 2015; Zetterberg et al., 2016), and baseline Aβ42 levels have been previously correlated with the pattern of atrophy in EOAD (Falgàs et al., 2020; Ossenkoppele et al., 2015b).

In this prospective study, we aim to describe the pattern of progressive atrophy in a well-characterized EOAD cohort over two years. We hypothesized that the longitudinal cortical loss in EOAD would follow a posterior gradient of cortical thinning and that the subcortical gray matter (GM) loss would extend beyond MTL structures. Secondly, we aim to define the relationship between baseline CSF levels of Aβ42, p-tau, t-tau and NfL, and the longitudinal rates of atrophy in EOAD. To confirm our results, we additionally analyze these parameters in EOAD and LOAD subjects from the Alzheimer's disease Neuroimaging Initiative (ADNI) database.

2. Methods

2.1. Participants

2.1.1. Discovery sample: Hospital Clínic of Barcelona cohort

We selected EOAD patients and age-matched healthy controls (HC) from a prospective cohort collected at the "Alzheimer's disease and Other Cognitive Disorders Unit" in Hospital Clínic, Barcelona (HCB).

Participants met the following inclusion criteria: having two available 3 T-MRI scans (one at baseline and one after 2 years), Mini Mental State Examination (MMSE) >= 15, available CSF biomarkers levels and multiple clinical and neuropsychological evaluations. Subjects with previous psychiatric or neurological conditions, autosomal dominant pattern of AD inheritance or gross brain pathology (i.e., stroke, tumor) were excluded. According to clinical and biomarker data (Jack et al., 2018), participants were classified in two groups:

- EOAD-HCB (N = 12): EOAD patients with AD core CSF biomarkers levels in the range suggesting the presence of AD neuropathology (A + T +) with neurodegeneration (N +). Patients also fulfilled NIA-AA diagnostic criteria for mild cognitive impairment (MCI) due to AD with high likelihood, or AD mild dementia with high evidence of AD pathophysiology process (Albert et al., 2011; McKhann et al., 2011). All subjects that fulfilled the inclusion criteria in this study presented an amnestic or multidomain neuropsychological profile at the time of the first MRI.
- HC (N = 19): research volunteers with cognitive performance within normative range and normal CSF levels of core AD biomarkers (A-T-N-).

This study was approved by HCB Ethics Committee and all the individuals gave written informed consent for their clinical data to be used for research purposes.

2.1.2. Replication sample: Alzheimer's disease Neuroimaging initiative (ADNI) cohort

To further investigate the interaction between CSF biomarkers levels and progressive GM loss, as well as a possible influence of age, we used two groups of patients obtained from the ADNI GO/2 database (adni.loni.usc.edu). The ADNI was launched in 2003 as a public–private partnership, led by Principal Investigator Michael W. Weiner, MD, with a primary goal to test whether different biomarkers can be combined to measure the progression of MCI and early AD. For up-to-date information, see www.adni-info.org.

The selection criteria for the EOAD-ADNI and LOAD-ADNI samples were identical to those of our discovery sample: a baseline diagnosis of MCI/AD, two 3 T-MRI scans with appropriate quality (baseline and at 2 years point), MMSE >= 15 and available CSF biomarkers at baseline. We selected patients with an A + T + N + profile in CSF and we excluded those with discordant Florbetapir-PET information. We included subjects < 65 years in the EOAD group (EOAD-ADNI: N = 14) and subjects >=75 years in the LOAD group (LOAD-ADNI: N = 55), to avoid a potential overlap between groups. In addition, we used available information in ADNI regarding CSF biomarkers rate of change at two years and baseline Florbetapir-PET Standardized Uptake Value Ratio (SUVR).

2.2. Cerebrospinal fluid biomarkers and APOE genotype

For the discovery cohort, all CSF samples were collected before the MRI scan except for one patient in EOAD-HCB and five subjects in HC. We used commercially available single-analyte enzyme-linked immunosorbent assay (ELISA) to determine levels of CSF Aβ42, p-tau, t-tau (INNOTEST, Fujirebio Europe N.V., Gent, Belgium) and NfL (IBL International, Hamburg, Germany). CSF samples in the ADNI cohort were collected after first MRI scan. Details regarding the CSF samples in the ADNI cohort are described elsewhere (Shaw et al., 2009). For the discovery cohort, we used the CSF Aβ42 (A), p-tau (T) and t-tau (N) cut-off values determined by our laboratory (Antonell et al., 2020). For the ADNI cohort, we used pre-defined cut-off points (Aβ42 < 980 pg/mL, p-tau > 21.8 pg/dl and t-tau > 245) to determine the ATN status.

APOE genotype was determined through the analysis of rs429358 and rs7412 by Sanger sequencing in the discovery cohort. *APOE* genotyping in ADNI has been outlined previously (Risacher et al., 2010). APOE status was analyzed according to the presence or absence of at

least one *APOE* ε4 allele.

2.3. Imaging acquisition

A 3 T Magnetom Trio Tim scanner (Siemens Medical Systems, Germany) at Hospital Clínic was used to collect the MR data of the discovery sample. A high-resolution 3D structural data set (T1-weighted, MP-RAGE, repetition time = 2,300 ms, echo time = 2.98 ms, 240 slices, field-of- view = 256 mm, voxel size = 1 × 1 × 1 mm) was acquired for all subjects at each time point. The ADNI brain MRI and Florbetapir-PET protocols have been reported in detail elsewhere (Jack et al., 2008; Landau et al., 2013).

2.4. Imaging processing

For the discovery sample, we first performed cortical reconstruction and volumetric segmentation of MRI scans using the longitudinal stream in FreeSurfer 6.0 (http://surfer.nmr.mgh.harvard.edu/). It creates a specific subject template in order to minimize the bias between time-points, leading to good reliability and reproducibility scores (Reuter et al., 2012). All the images in this study were visually inspected and manually corrected when needed.

Using the FreeSurfer longitudinal stream, we obtained cortical thickness (CTh) maps and subcortical volumes at each time-point. We used the symmetrized percent change (spc) to evaluate longitudinal changes in CTh, calculated as the rate of thickness change (CTh at time2 – CTh at time1) divided by the average thickness ((CTh at time2 + CTh at time1)/2). Before statistics, all CTh maps were registered to a common space and smoothed using a full-width at half maximum (FWHM) kernel of 15 mm. In addition, we obtained global CTh measures for each hemisphere (mean CTh across all the vertices) and summary measures within the atlas-based parcellations available in FreeSurfer (34 cortical regions in each hemisphere) (Desikan et al., 2006).

For the subcortical structures, we obtained volumetric measures at baseline and at two years for the 23 atlas-based subcortical GM regions available (Seidman et al., 1997) and we calculated the spc, using the same method described for the CTh maps.

For the replication samples, we downloaded the summary table of longitudinal measurements for subcortical volumes and CTh, which have been calculated within the ADNI pipeline. We calculated the spc at two years point as previously described. In addition, we downloaded the summary table of SUVR calculations for amyloid-PET.

2.5. Statistical analysis demographics, clinical data and CSF biomarkers levels

To compare differences between groups at baseline, the Mann-Whitney *U* test was used for continuous variables and the Fisher's exact tests for the sex and *APOE* ε4 distributions. In addition, we performed a cross-correlation correlation analysis between the CSF biomarkers levels in each of the different AD samples. All the statistical analyses were conducted using R version 4.0.2 (http://www.R-project.org/)

2.6. Cortical thickness analysis

For the discovery sample (EOAD-HCB), we used tools available in FreeSurfer to obtain vertexwise differences between groups, using different general linear model (GLM) designs. We obtained group CTh differences at baseline, as well as differences in CTh spc maps, using age and sex as covariates. Information on baseline atrophy was included to describe which regions were preserved or atrophied at baseline and presented (or not) atrophy over two years. All maps were corrected for multiple comparisons using a permutation-based method, as

implemented in Freesurfer. This method corrects for family-wise error (FWE) while accounting for the distribution of the data using Monte Carlo permutations at the cluster level. Significance level for the group differences was set at p < 0.01. In addition, we used global CTh measures for each hemisphere and atlas-based parcellations to further study cortical differences across groups, using Mann-Whitney *U* test. To better compare our results across cohorts, and to explore a possible bias results towards regions that might have severe atrophy at baseline, we also studied differences in longitudinal cortical loss across groups using the rate of change (CTh at time2 - CTh at time1/Time 2 - Time 1).

Within the EOAD-HCB group, we performed correlations between initial CSF biomarker levels (Aβ42, p-tau, t-tau, and NfL) and whole CTh spc maps. The resulting correlation maps were corrected for multiple comparisons as stated above and thresholded at p < 0.05. After the correlation analysis between the spc map and the initial CSF levels, we used Spearman's coefficients to correlate separately the spc of the regions that were identified in the previous clusters and the corresponding levels of CSF biomarkers (for interpretation purposes). We then correlated separately the spc of these regions with CSF biomarker levels in the EOAD-ADNI and the LOAD-ADNI groups. In addition, to better understand this relationship, we performed the same analysis using the measures of the regions that showed atrophy in EOAD-HCB at baseline. We also correlated CTh spc with initial CSF biomarkers levels using the full sample of EOAD-HCB and HC subjects in the analysis. Finally, we performed a cross-correlation analysis between the CSF biomarkers in the different AD samples. Since we found differences between the interval between the first MRI and the lumbar puncture in EOAD-HCB, EOAD-ADNI and LOAD-ADNI, we tested a possible influence of this interval in CSF levels or the spc decline.

2.7. Subcortical volume analysis

For the discovery sample, we used the Mann-Whitney *U* test to calculate group differences in volume at the time of the first scan and the differences in spc longitudinally. For volume analyses, significance level was set at p < 0.002, which was the result of adjusting an initial p level of 0.05 to account for all the independent tests assessed, according to the Bonferroni criteria for multiple comparisons correction. In addition, we repeated the cross-sectional analysis after intracranial volume adjustment. The longitudinal analysis for subcortical GM loss was also repeated using the rate of change as previously described.

We then used Spearman's coefficients to correlate initial CSF biomarker levels and the spc in the structures that showed significant longitudinal atrophy. Later, we repeated the analysis using the previously identified significant regions but in the ADNI cohort. Also, the volume of the structures that exhibited baseline atrophy was correlated with initial biomarkers level and the spc was correlated including EOAD-HCB and HC in a single correlation analysis. The influence of the interval between MRI scan and lumbar puncture in spc was also investigated.

3. Results

3.1. EOAD-HCB cohort: Baseline demographics, clinical data and CSF biomarkers levels

Demographics, MMSE scores, *APOE* genotype and CSF biomarkers levels are shown in Table 1. As expected from the groups' conformation, EOAD-HCB presented lower Aβ42 and higher t-tau, p-tau and NfL levels and scored worse in MMSE than HC. There were no differences between groups in age at the first MRI scan, time between scans, time between the first MRI scan and the lumbar puncture, sex or *APOE* ε4 status. In addition, we found that higher levels of Aβ42, p-tau and NfL correlated with higher levels of t-tau in EOAD-HCB. P-tau also correlated with NfL (p < 0.05, Supplementary Fig. 1).

Table 1
Demographic, clinical characteristics, and CSF biomarkers levels for groups included in analysis.

Variable	EOAD-HCB	HC	EOAD-ADNI	LOAD-ADNI
N	12	19	14	55
Female/Male	8/4	16/3	8/6	24/31
Age at onset, years	57.25(4.86)	N/A	NE	NE
Age at first MRI, years	60.64 (4.58)	57.96 (4.68)	60.7 (3.38)	79.41 (3.45)‡
Time to second MRI, years	1.99 (0.17)	2.02 (0.25)	2.06 (0.1)†	2.08 (0.09)‡
Time between MRI and CSF, years	0.66 (1.17)	1.15 (1.05)	0.13 (0.13)†	0.08 (0.05)‡
APOE ε4 carriers/ non carriers	3/9	3/16	13/1†	21/34‡
MMSE, mean	20.83 (3.43)*	29.27 (1.06)	26.07 (3.08)†	26.55 (2.73)‡
Aβ42, mean pg/mL	387.65 (73)*	892.26 (217.88)	653.14 (181.43)	674.72 (166.85)
p-tau, mean pg/mL	103.65 (24.29)*	53.27 (11.20)	45.18 (15.21)	37(16.5)
t-tau, mean pg/mL	740.28 (282.44)*	227.29 (50.91)	438.89 (127.25)	364.54 (145.53)
NfL , mean pg/mL	914.94 (219)*	416.50 (109.12)	NE	NE

NOTE. Data are presented as mean (standard deviation). *p < 0.05 for the comparisons between EOAD-HCB and HC; †p < 0.05 for the comparisons between EOAD-HCB and EOAD-ADNI; ‡p < 0.05 for the comparisons between EOAD-HCB versus LOAD-ADNI. Abbreviations: EOAD, early-onset AD; HCB, Hospital Clinic; HC, healthy controls; LOAD, late-onset AD; N/A, not applicable; NE, not evaluated; MRI, Magnetic resonance imaging; CSF; cerebrospinal fluid; MMSE, Mini-Mental State Examination; Aβ42, amyloid β42; p-tau, phosphorylated tau; t-tau, total tau; NfL, neurofilament light chain.

3.2. EOAD-ADNI cohort: Baseline demographics, clinical data and CSF biomarkers levels

Data from the EOAD-ADNI and LOAD-ADNI samples are presented in Table 1. Compared to EOAD-HCB, we found no differences in age at first MRI scan in the EOAD-ADNI, while the LOAD-ADNI group was older, as expected. Compared to EOAD-HCB, EOAD-ADNI and LOAD-ADNI showed differences in MMSE score, proportion of *APOE* ε4 carriers, time between scans and the time between the first MRI scan and the lumbar puncture. No sex differences were found. Higher CSF levels of p-tau correlated with higher t-tau levels in EOAD-ADNI and LOAD-ADNI (p < 0.05, Supplementary Fig. 2).

3.3. EOAD-HCB baseline analyses

3.3.1. Cortical thickness

The EOAD-HCB group showed lower CTh than HC in global CTh of left and right hemispheres (p = 0.00072 and p = 0.0042, respectively), with no differences between them (p = 0.55). With the vertex-wise analyses, we found a pattern of reduced CTh in EOAD-HCB compared to HC (p < 0.01 cluster-wise corrected, Fig. 1A). These differences comprised the bilateral precuneus, the posterior and isthmus cingulate regions, areas surrounding the temporoparietal junction - including the bilateral supramarginal, the superior and inferior parietal, banks of the superior temporal sulcus (bankssts) - as well as the superior, middle and inferior temporal regions. These differences also extended into the right lateral occipital cortex. However, the EOAD-HCB group did not show differences in CTh in the MTL, the temporal pole or the frontal lobe compared to HC.

When analyzing the CTh of atlas-based parcellations, we found that the bilateral middle temporal, the precuneus and the inferior parietal regions showed the greatest reduction in CTh in EOAD-HCB compared to HC, in addition to the left inferior temporal and left supramarginal (all p < 0.00074, Supplementary Table 1).

3.3.2. Subcortical volumes

EOAD-HCB group showed lower volume in bilateral hippocampus and amygdala and greater volume of inferior-lateral ventricles when compared to HC (all p < 0.002; Fig. 2A, Supplementary Table 2). Results did not differ after adjusting for total intracranial volume.

3.4. EOAD-HCB longitudinal analysis

#### 3.4.1. Longitudinal changes in cortical thickness

EOAD-HCB showed longitudinal cortical thinning in posterior rather than anterior regions compared to HC (p < 0.01 cluster-wise corrected; Fig. 1B). Areas affected at baseline continued changing over 2 years and additional longitudinal atrophy was found in the bilateral MTL, including the entorhinal and parahippocampal regions, fusiform, insular, lateral occipital and lingual regions.

Using global CTh measures, we observed greater longitudinal CTh
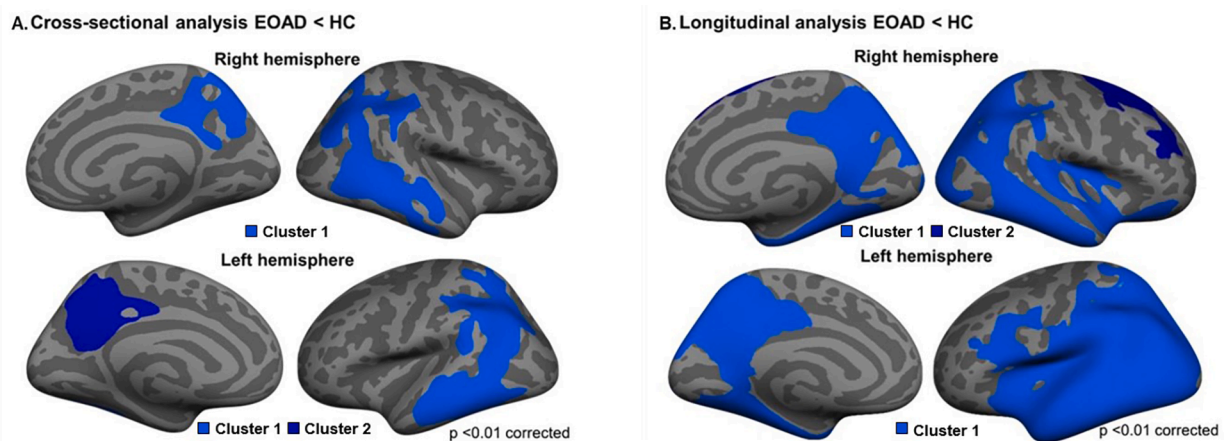
Fig. 1. Vertex-wise maps of the differences between EOAD-HCB and HC in (A) cortical thickness at baseline and (B) cortical thickness spc at two years. Significant clusters of gray matter loss are shown in light and dark blue, EOAD < HC with a corrected p < 0.01. The results are represented on the fsaverege model. At baseline (A), the EOAD-HCB participants exhibited lower CTh than HC in three clusters, one in the right hemisphere (size = 13,262.72 mm²) and two in the left hemisphere (light blue = 3,182.41 mm² and dark blue = 1,2555.52 mm²). At two years (B), EOAD-HCB showed lower spc in three cluster, two in the right hemisphere (dark blue = 3,777.76 mm² and light blue = 30,742.5 mm²) and one in the left hemisphere (size = 44424.55 mm²). Abbreviations: EOAD, early-onset AD; HCB, Hospital Clinic Barcelona; HC, healthy controls; CTh, cortical thickness; spc, symmetrized percent change. (For interpretation of the references to colour in this figure legend, the reader is referred to the web version of this article.)

A. Subcortical volume at baseline

B. Subcortical volume spc
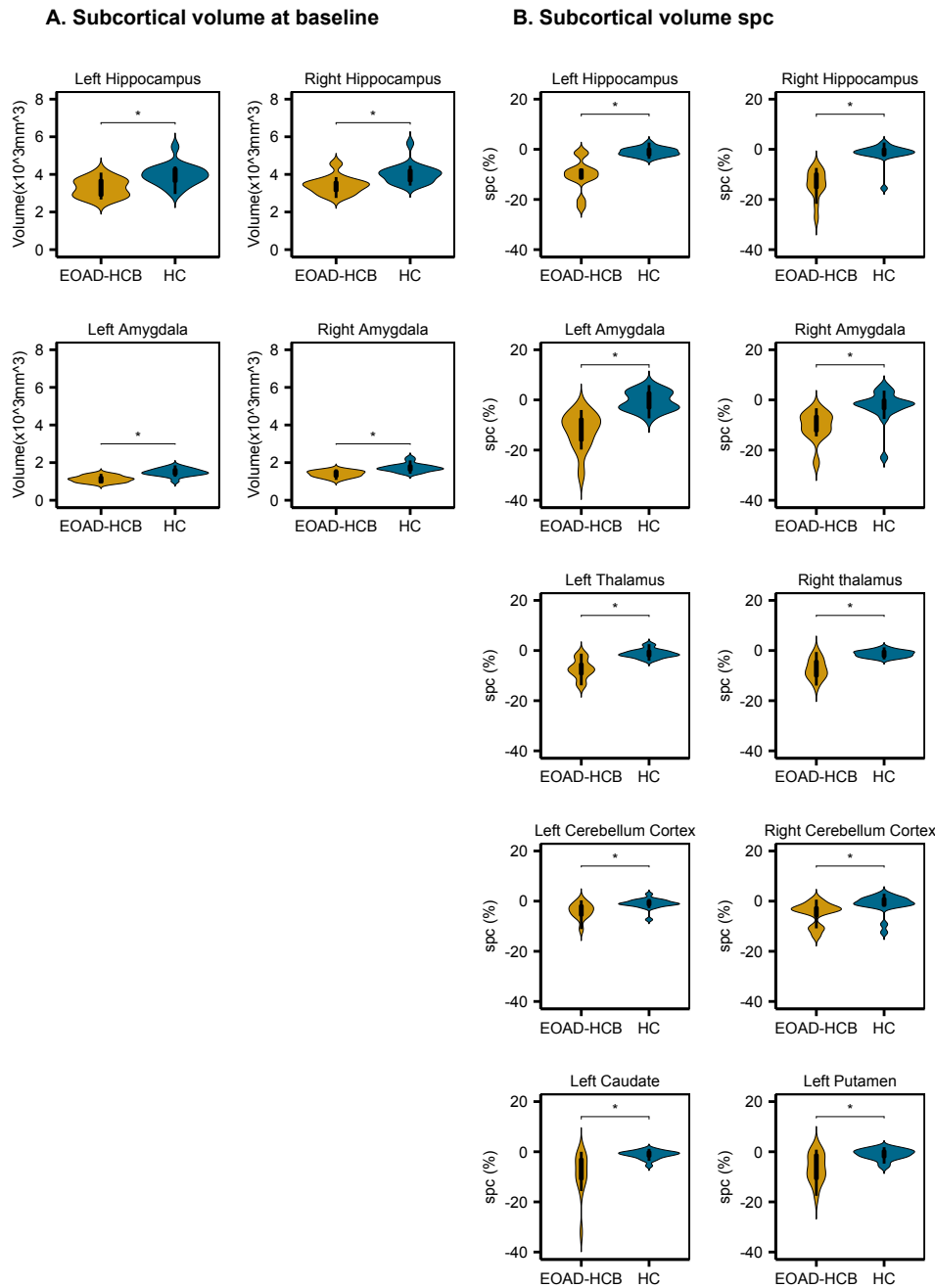
Fig. 2. Significant differences between EOAD-HCB and HC in (A) subcortical gray matter volume at baseline and (B) subcortical volume spc at two years. *p-values < 0.002. Statistical analyses have been performed with Mann-Whitney *U* test and corrected for multiple comparisons with the Bonferroni's method. Abbreviations: EOAD, early-onset AD; HCB, Hospital Clinic Barcelona; HC, healthy controls; spc, symmetrized percent change.

loss in both hemispheres in EOAD-HCB compared to HC (p < 0.000001), with no differences between hemispheres (p = 0.59). However, we observed asymmetries in the topography of longitudinal atrophy in the spc maps. In the left hemisphere, cortical loss involved language-related areas such as the pars opercularis and the transverse temporal gyri, while right atrophy spread further into the visual cortex (cuneus) and prefrontal areas. Compared to HC, the greatest rates of cortical thinning in EOAD-HCB were found in the bilateral entorhinal, right fusiform, left precuneus and bilateral parahippocampal regions (all p < 0.00074; Table 2, Supplementary Table 3). When using the rate of change as measure of longitudinal CTh loss results did not change (all p < 0.00074, Supplementary Table 4).

3.4.2. Symmetrized percent change in subcortical volume

In two years, the EOAD-HCB group showed volume loss in regions beyond the MTL, including the bilateral hippocampus, amygdala, thalamus, cerebellum GM, and left caudate and putamen regions. This loss was accompanied by a bilateral enlargement in the lateral and inferior-lateral ventricles (all p < 0.002, Bonferroni-corrected; Fig. 2B, Supplementary Table 5). The greatest reductions were observed in the bilateral hippocampus, amygdala, thalamus and left caudate regions (Table 2). Using the rate of change instead of the spc, the subcortical regions that exhibited longitudinal atrophy remained the same (all p < 0.002, Supplementary Table 6), except the left pallidum (p = 0.0025).

Table 2
Symmetrized percent change (%) of regions that exhibited greater longitudinal atrophy.

Region	EOAD-HCB	HC	p value
Right entorhinal	−12.5(4.3)	−0.4(2.9)	0.00000005
Left entorhinal	−12.1(5.3)	−0.6(1.9)	0.00000003
Right fusiform	−8.9(4.7)	−0.1(1.8)	0.00000009
Left precuneus	−8.6(4.5)	−0.7(2.2)	0.00000032
Right parahippocampal	−8.5(6.4)	0.1(1.8)	0.000011
Left parahippocampal	−8.2(4.2)	0(2.5)	0.0000048
Right hippocampus	−14(5.9)	−1.5(3.7)	0.000001
Left Amygdala	−12.3(7.3)	−0.5(3.8)	0.0000002
Left hippocampus	−10.4(6.3)	−1(1.7)	0.0000084
Right amygdala	−10.4(5.8)	−2.2(6)	0.0000184
Left Caudate	−8.9(8.8)	−1.2(1.6)	0.0002964
Left Thalamus	−7.3(3.9)	−1.2(1.7)	0.0000084
Right thalamus	−7.3(3.9)	−1.3(1.3)	0.0000064

NOTE. Data are presented as mean (standard deviation). Abbreviations: EOAD, early-onset AD; HCB, Hospital Clinic; HC, healthy controls. Additional information can be found in Supplementary.

3.5. Correlation between baseline and longitudinal GM changes and initial CSF biomarkers

3.5.1. Baseline and longitudinal CTh changes and initial CSF biomarkers in EOAD-HCB cohort

At baseline, no correlations were found between the regions that exhibited cortical loss and the CSF biomarkers levels in EOAD-HCB (p > 0.05). At two years, initial CSF Aβ42 levels showed a negative correlation with longitudinal CTh loss in areas of the right hemisphere (corrected p < 0.05; Fig. 3A). CSF p-tau, t-tau or NfL levels did not yield any significant results (p > 0.05).

High levels of Aβ42 in EOAD patients correlated with accelerated cortical thinning in two clusters, covering the right superiorparietal, precuneus, lingual and isthmus cingulate cortices (cluster 1: ρ = -0.85); and the right precuneus, posterior cingulate and paracentral cortices (cluster 2: ρ = -0.83). When we studied the spc within these regions, as obtained with the atlas-based measures, high CSF Aβ42 levels in EOAD-HCB correlated with faster cortical thinning in the right precuneus (ρ = -0.78, p = 0.0047) and superior parietal regions (ρ = -0.59, p = 0.049) (Fig. 3B).

In addition, when including EOAD-HCB and HC subjects in a single correlation analysis, we found that baseline levels of CSF biomarkers (Aβ42, t-tau, p-tau, NfL) correlated with the CTh spc measures in the majority of cortical regions. In this case, higher CSF Aβ42 levels were correlated with less atrophy over two years in all regions that showed longitudinal atrophy, except left cuneus and left putamen; higher t-tau, p-tau and NfL levels were correlated with higher longitudinal atrophy in all regions (all p < 0.05, Supplementary Table 7).

3.5.2. Baseline and longitudinal changes in subcortical volumes and initial CSF biomarkers in EOAD-HCB cohort

In EOAD-HCB, higher initial CSF NfL levels were correlated with higher volume of the left lateral ventricle at baseline (ρ = 0.59, p = 0.049; Supplementary Fig. 3). In contrast, higher baseline CSF t-tau levels correlated with greater volume loss over two years in left amygdala (ρ = -0.601, p = 0.042; Fig. 3B (ρ = 0.59, p = 0.049; Supplementary Fig. 3). CSF Aβ42 or p-tau levels did not showed any significant correlation with baseline measures or longitudinal atrophy. On the other hand, when including EOAD-HCB and HC in the analysis, initial CSF biomarkers correlated with longitudinal atrophy. As expected, higher CSF Aβ42 were correlated with less atrophy over two years, except left putamen; higher t-tau levels were correlated with higher longitudinal atrophy in all the regions except left caudate; higher p-tau levels were correlated with higher longitudinal atrophy except left cerebellum cortex; higher NfL were correlated with higher longitudinal atrophy in all the regions (all p < 0.05, Supplementary Table 8).

3.5.3. Longitudinal GM changes and initial CSF biomarkers in ADNI cohort

In EOAD-ADNI but not in LOAD-ADNI, higher CSF Aβ42 levels at baseline correlated with accelerated cortical loss over the next two years in the right precuneus (ρ = -0.6, p = 0.026) and right superior parietal regions (ρ = -0.54, p = 0.048) (Fig. 3B). In contrast, we found that high CSF t-tau values at baseline correlated with greater volume loss in the left amygdala in LOAD-ADNI (ρ = -0.374, p = 0.0051; Fig. 3B), but not in EOAD-ADNI.

The available 18F-AV-45 (Florbetapir) PET SUVR in right precuneus and superior parietal regions, parietal lobes and whole brain did not correlated with the atrophy rates of the above regions in EOAD-ADNI (n = 14, Supplementary Table 9). In EOAD-ADNI (n = 8), the annualized rate of change in CSF Aβ42 levels (mean = -30.6, standard deviation = 61.8) did not show significant correlation with right precuneus or superiorparietal spc. Furthermore, the CSF t-tau annualized rate of change (mean = 3.9, standard deviation = 28) was also not correlated with left amygdala (p > 0.05) in LOAD-ADNI (n = 33). No significant correlations were observed between the interval between the first MRI and the lumbar puncture and CSF levels or spc decline, neither in EOAD-HCB nor in EOAD-ADNI/LOAD-ADNI (p > 0.05).
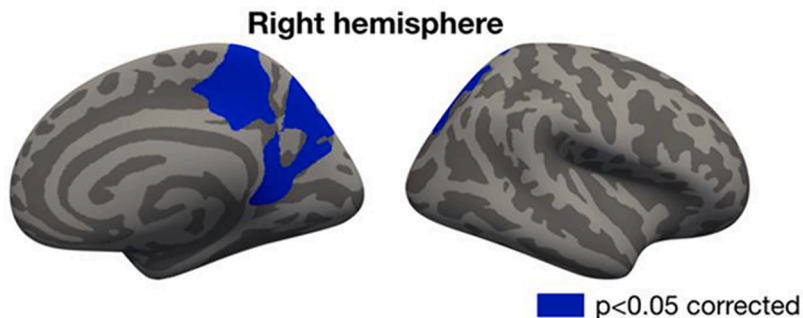
4. Discussion

We performed a prospective 3T-MRI study to track CTh and GM volume changes in EOAD. First, we analyzed the pattern of initial atrophy in EOAD to describe which regions were preserved or atrophied at baseline and which presented longitudinal atrophy. We showed that posterior cortices, together with the hippocampus and the amygdala, were the most affected regions at the time of diagnosis. The longitudinal analysis at 2 years showed that progressive atrophy spreads throughout the neocortex with a posterior-to-anterior gradient and beyond the initial subcortical structures. Finally, we observed that, within the pathological range, initial CSF Aβ42 levels closer to the to the normality threshold were associated with accelerated cortical loss in posterior regions in EOAD whereas higher baseline t-tau levels correlated with greater rates of volume loss in MTL subcortical structures in EOAD and LOAD samples.
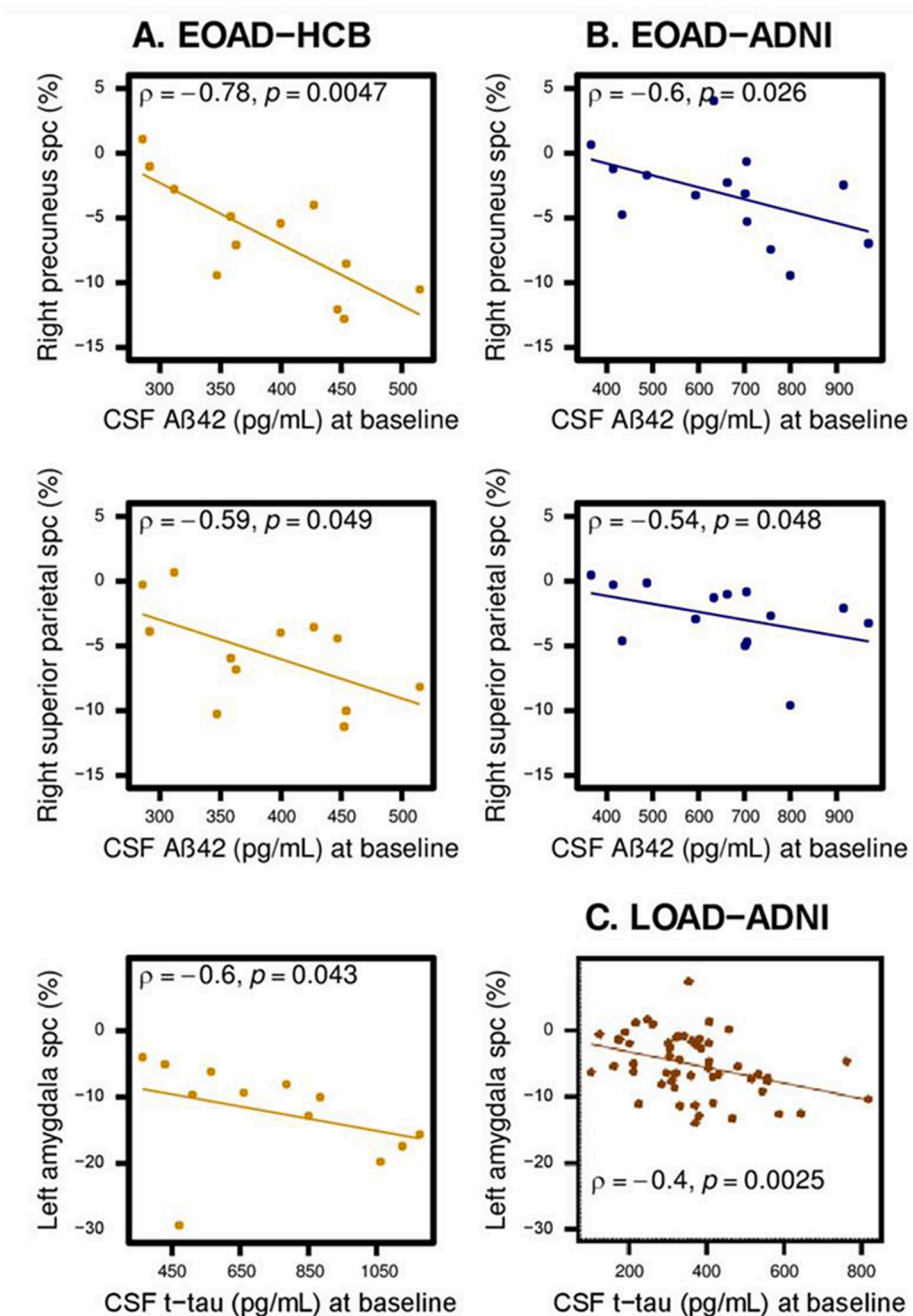
At baseline, we described lower CTh in EOAD in the bilateral parietal, precuneus, and posterior cingulate as well as in the lateral temporal lobes and right occipital cortices. Previous cross-sectional MRI studies have also found widespread brain atrophy in EOAD, particularly in parietotemporal areas when compared to LOAD (Aziz et al., 2017; Falgàs et al., 2020; Harper et al., 2017; Möller et al., 2013; Ossenkoppele et al., 2015a). We found that the thickness of the entorhinal and parahippocampal cortices was preserved at the time of diagnosis, in consonance with studies describing greater pathological burden (Murray et al., 2011; Whitwell et al., 2012) and greater Tau deposit outside the MTL at younger ages (Joie et al., 2020; Schöll et al., 2017). In addition, our results describing lower volumes in the hippocampus and amygdala in EOAD also agree with previous studies on subcortical structures (Cavedo et al., 2014; van de Pol et al., 2006).

Amyloid deposits are first observed in the isocortex and then in subcortical structures while NFTs accumulate in the MTL before neocortical involvement (Braak and Braak, 1991; Hyman et al., 2012). We found that EOAD patients show atrophy in isocortical areas whereas the entorhinal/parahippocampal cortices were spared at early stages. This suggests a specific pattern of atrophy for patients with EOAD in which the MTL might be less influenced by other processes associated with aging (Savva et al., 2009). The posterior-to-anterior gradient is consistent with previous longitudinal MRI studies analyzing structural changes according to age at onset (Fiford et al., 2018; Joie et al., 2020; Thijssen et al., 2020). In subjects without biomarkers characterization, Cho et al. found cortical loss throughout the cortex over three years (Cho et al., 2013a) whereas Migliaccio et al. found that volume loss spread from the hippocampus and parietotemporal cortices to the precuneus and isthmus cingulate regions, and the MTL cortices were spared over

A. Correlation between CTh spc and CSF Aβ42

Right hemisphere

p<0.05 corrected

Fig. 3. (A) Vertex-wise maps of correlations between the cortical thickness spc and baseline cerebrospinal fluid Aβ42 levels in EOAD-HCB (p < 0.05 cluster-wise corrected; cluster1 size = 3461.18 mm^2; cluster2 size = 1891.24 mm^2). (B) Significant correlations between the regional rates of gray matter atrophy in EOAD-HCB, EOAD-ADNI and LOAD-ADNI and the baseline cerebrospinal fluid biomarkers levels. Abbreviations: CTh, cortical thickness; spc, symmetrized percent change; Aβ42, amyloid β42; EOAD, early-onset AD; HCB, Hospital Clinic Barcelona; ADNI, Alzheimer's disease neuroimaging initiative; t-tau, total tau.

B. Correlation between rates of atrophy and CSF biomarkers in HCB and ADNI samples

one year (Migliaccio et al., 2015). Volume loss in subcortical structures beyond the MTL is in line with previous reports (Cho et al., 2013b; Fiford et al., 2018) and some authors even suggest specific pathomechanisms for subcortical atrophy in EOAD (Lee et al., 2020).

Although the MTL presented the greatest rates of CTh and subcortical GM loss at the longitudinal level, atrophy was only detectable in subcortical structures at the time of diagnosis. The precuneus, isthmus cingulate, and lateral parietotemporal regions had reduced CTh at the time of the diagnosis and accelerated cortical loss over two years. Here, we reinforce the idea that the posterior associative regions might better capture cortical loss in EOAD than the MTL (Hamelin et al., 2015). The precuneus and posterior cingulate are early sites of amyloid deposition and had been implicated in changes of the default mode network at early AD phases (Palmqvist et al., 2017). In addition to an age effect, the more focally posterior GM changes in the neocortex could be influenced by the low number of *APOE* ε4 carriers in our cohort (Mattsson et al., 2018).

Higher CSF Aβ42 levels, within pathological range, were associated with faster cortical loss in precuneus and superior parietal cortices in the two EOAD cohorts, but not in LOAD subjects. CSF Aβ42 levels have been related to EOAD GM loss in cross-sectional studies (Falgàs et al., 2020; Ossenkoppele et al., 2015b). Although AD biomarkers of neurodegeneration become abnormal after amyloid biomarkers (Jack et al., 2018), rates of atrophy might accelerate before the conventional thresholds of CSF Aβ42 positivity (Insel et al., 2016). In preclinical stages, transitional CSF Aβ42 values are related to increased CTh in temporoparietal and precuneus regions (Fortea et al., 2011) and a reduction in the rates of brain atrophy is followed by an acceleration of cortical loss once CSF Tau levels increase (Pegueroles et al., 2017). Here, we found a counterintuitive correlation between amyloid and CTh spc for the two EOAD samples. One possible explanation could be that the rates of cortical loss observed in subjects close to the Aβ42 positivity threshold reflect greater inflammation in vulnerable regions due to accelerated deposit of amyloid once levels become abnormal (Kreisl et al., 2013; Ossenkoppele et al., 2012). Amyloid pathology precedes and activates microglia (Parbo et al., 2018) and the dual peak hypothesis of neuroinflammation in AD suggests that an early peak in activated microglia is initially protective, attempting to remove Aβ, whereas a later peak is detrimental (Fan et al., 2017). On the other hand, higher inflammation in medial temporal regions and the hippocampus has been negatively associated with hippocampal volume in [11C]PK11195-PET and MRI studies (Femminella et al., 2016). Here, initial CSF Aβ42 levels might correlate with neuroinflammation in EOAD, predicting an acceleration of atrophy due to activated microglia. In addition, in our cohort, EOAD subjects that exhibited higher pathological levels of Aβ42 also presented higher t-tau levels, maybe suggesting higher degree of neurodegeneration. Our results cannot indicate cause-effect relationships but suggest that amyloid-dependent neurodegeneration might be related to the observed progressive cortical thinning in EOAD subjects. Both EOAD samples showed differences in the proportion of *APOE* carriers and MMSE scores. This suggests that the relationship between CSF Aβ42 levels and the cortical thinning could be observed in EOAD patients with MCI and mild dementia regardless of the *APOE* genotype. Although previous studies have reported a dose-dependent CSF Aβ42 effect in APOE ε4 LOAD patients, the available evidence exploring this effect in EOAD is limited (Kaur et al., 2020). In addition, previous studies have reported that the correlation between amyloid-PET and cortical thickness is typically poor (Whitwell et al., 2018). Although both CSF Aβ42 and amyloid PET are valid biomarkers of brain Aβ-plaque load, our findings, as whole, contribute to highlight the complex relationships at the regional level between atrophy and amyloid biomarkers. Novel image coregistration techniques might improve the sensitivity of the detection of a correlation between amyloid PET and longitudinal atrophy in MRI (Pillai et al., 2020).

We also observed that NfL or t-tau might be associated with subcortical volume loss independently of subjects' age. As previously proposed across the AD continuum (Fjell et al., 2010), we observed that higher t-tau levels at baseline correlated with accelerated atrophy in the left amygdala in EOAD and LOAD, although not replicated in the two EOAD samples. In addition, we observed that higher NfL levels at baseline were related to cross-sectional ventricular enlargement. T-tau/ NfL levels have shown low correlation with cortical thickness, regardless of the time interval, and these biomarkers might be more related with other neurodegeneration processes rather than cortical thinning (Boerwinkle et al., 2021). Despite of CSF t-tau and NfL levels represent N biomarkers, t-tau might reflect Aβ42-dependent subcortical atrophy while NfL might indicate neurodegeneration independently of amyloid pathology (Tarawneh et al., 2015; Zetterberg et al., 2016). On the other hand, we found that p-tau was not correlated with MRI atrophy. However, p-tau was highly correlated with t-tau and NfL levels, supporting the notion that p-tau is related with the abnormal phosphorylated state of tau in AD whereas t-tau reflects the intensity of brain damage (Jack et al., 2018). Still, p-tau, and the rest of CSF biomarkers used in this study, correlated with the degree of atrophy over time when EOAD and healthy subjects were analyzed together. Whether CSF biomarkers represent a marker of future atrophy associated with underlying pathology must be assessed in further studies.

Similar to other EOAD studies, our main limitation is the relatively small sample size, which might limit the power to detect further differences in atrophy or correlations between CSF biomarkers and atrophy. For this reason, we replicated the correlation analysis in two independent cohorts. The selection criteria in the ADNI cohort might account for the observed differences between EOAD-ADNI/LOAD-ADNI and EOAD patients in memory clinic setting, exemplified by higher number of *APOE* ε4 + cases and better cognitive status in ADNI. Another strength of our study is the use of CTh measures that may reflect changes more specific to AD than the previous volumetric analysis which are more influenced by the effect of aging or other pathologies on white matter loss (Feczko et al., 2009). Studies in larger EOAD cohorts and selecting preclinical subjects can expand our results and define the sequence of early atrophy.

5. Conclusion

We characterized progressive cortical thinning and subcortical volume loss in biologically well-characterized EOAD patients and young controls. We showed that posterior cortices, hippocampus and amygdala capture better the progressive atrophy in EOAD at early stages than the MTL. Our study narrows the field of brain areas for disease tracking, providing a valuable prior constraint on future hypothesis testing. More research is required to understand age-related mechanisms for atrophy spreading and the relationship between the pattern of atrophy and CSF biomarkers.

CRediT authorship contribution statement

José Contador: Conceptualization, Methodology, Investigation, Formal analysis, Writing – original draft, Visualization, Data curation, Resources. **Agnès Pérez-Millán:** Methodology, Software, Formal analysis, Writing - review & editing. **Adrià Tort-Merino:** Writing - review & editing. **Mircea Balasa:** Writing - review & editing. **Neus Falgàs:** Writing - review & editing. **Jaume Olives:** Writing - review & editing. **Magdalena Castellví:** Writing - review & editing. **Sergi Borrego-Écija:** Writing - review & editing. **Beatriz Bosch:** Writing - review & editing. **Guadalupe Fernández-Villullas:** Writing - review & editing. **Oscar Ramos-Campoy:** Writing - review & editing. **Anna Antonell:** Writing - review & editing. **Nuria Bargalló:** Writing - review & editing. **Raquel Sanchez-Valle:** Writing - review & editing. **Roser Sala-Llonch:** Conceptualization, Methodology, Software, Formal analysis, Investigation, Resources, Writing - review & editing, Visualization, Supervision. **Albert Lladó:** Conceptualization, Methodology, Investigation, Resources, Data curation, Writing - review & editing, Supervision, Funding acquisition, Project administration. : .

Declaration of Competing Interest

Appendix A. Supplementary data

Supplementary data to this article can be found online at https://doi.org/10.1016/j.nicl.2021.102804.

References

Albert, M.S., DeKosky, S.T., Dickson, D., Dubois, B., Feldman, H.H., Fox, N.C., Gamst, A., Holtzman, D.M., Jagust, W.J., Petersen, R.C., Snyder, P.J., Carrillo, M.C., Thies, B., Phelps, C.H., 2011. The diagnosis of mild cognitive impairment due to Alzheimer's disease: Recommendations from the National Institute on Aging-Alzheimer's Association workgroups on diagnostic guidelines for Alzheimer's disease. Alzheimer's & Dementia 7 (3), 270–279.

Antonell, A., Tort-Merino, A., Ríos, J., Balasa, M., Borrego-Écija, S., Auge, J.M., Muñoz-García, C., Bosch, B., Falgàs, N., Rami, L., Ramos-Campoy, O., Blennow, K., Zetterberg, H., Molinuevo, J.L., Lladó, A., Sánchez-Valle, R., 2020. Synaptic, axonal damage and inflammatory cerebrospinal fluid biomarkers in neurodegenerative dementias. Alzheimer's & Dementia 16 (2), 262–272.

Aziz, A.-L., Giusiano, B., Joubert, S., Duprat, L., Didic, M., Gueriot, C., Koric, L., Boucraut, J., Felician, O., Ranjeva, J.-P., Guedj, E., Ceccaldi, M., 2017. Difference in imaging biomarkers of neurodegeneration between early and late-onset amnestic Alzheimer's disease. Neurobiol. Aging 54, 22–30. https://doi.org/10.1016/j.neurobiolaging.2017.02.010.

Boerwinkle, A.H., Wisch, J.K., Chen, C.D., Gordon, B.A., Butt, O.H., Schindler, S.E., Sutphen, C., Flores, S., Dincer, A., Benzinger, T.L.S., Fagan, A.M., Morris, J.C., Ances, B.M., 2021. Temporal Correlation of CSF and Neuroimaging in the Amyloid-Tau-Neurodegeneration Model of Alzheimer Disease. Neurology 97 (1), e76–e87. https://doi.org/10.1212/wnl.0000000000012123.

Braak, H., Braak, E., 1991. Neuropathological stageing of Alzheimer-related changes. Acta Neuropathol 82 (4), 239–259. https://doi.org/10.1007/BF00308809.

Cavedo, E., Pievani, M., Boccardi, M., Galluzzi, S., Bocchetta, M., Bonetti, M., Thompson, P.M., Frisoni, G.B., 2014. Medial temporal atrophy in early and late-onset Alzheimer's disease. Neurobiol. Aging 35 (9), 2004–2012. https://doi.org/10.1016/j.neurobiolaging.2014.03.009.

Cho, H., Jeon, S., Kang, S.J., Lee, J.-M., Lee, J.-H., Kim, G.H., Shin, J.S., Kim, C.H., Noh, Y., Im, K., Kim, S.T., Chin, J., Seo, S.W., Na, D.L., 2013a. Longitudinal changes of cortical thickness in early- versus late-onset Alzheimer's disease. Neurobiol. Aging 34 (7), 1921.e9–1921.e15. https://doi.org/10.1016/j.neurobiolaging.2013.01.004.

Cho, H., Seo, S.W., Kim, J.-H., Kim, C., Ye, B.S., Kim, G.H., Noh, Y., Kim, H.J., Yoon, C. W., Seong, J.-K., Kim, C.-H., Kang, S.J., Chin, J., Kim, S.T., Lee, K.-H., Na, D.L., 2013b. Changes in subcortical structures in early- versus late-onset Alzheimer's disease. Neurobiol. Aging 34 (7), 1740–1747. https://doi.org/10.1016/j.neurobiolaging.2013.01.001.

Desikan, R.S., Ségonne, F., Fischl, B., Quinn, B.T., Dickerson, B.C., Blacker, D., Buckner, R.L., Dale, A.M., Maguire, R.P., Hyman, B.T., Albert, M.S., Killiany, R.J., 2006. An automated labeling system for subdividing the human cerebral cortex on MRI scans into gyral based regions of interest. NeuroImage 31 (3), 968–980. https://doi.org/10.1016/j.neuroimage.2006.01.021.

Falgàs, N., Ruiz-Peris, M., Pérez-Millan, A., Sala-Llonch, R., Antonell, A., Balasa, M., Borrego-Écija, S., Ramos-Campoy, O., Augé, J.M., Castellví, M., Tort-Merino, A., Olives, J., Fernández-Villullas, G., Blennow, K., Zetterberg, H., Bargalló, N., Lladó, A., Sánchez-Valle, R., 2020. Contribution of CSF biomarkers to early-onset Alzheimer's disease and frontotemporal dementia neuroimaging signatures. Hum. Brain Mapp. 41 (8), 2004–2013. https://doi.org/10.1002/hbm.24925.

Falgàs, N., Tort-Merino, A., Balasa, M., Borrego-Écija, S., Castellví, M., Olives, J., Bosch, B., Férnandez-Villullas, G., Antonell, A., Augé, J.M., Lomeña, F., Perissinotti, A., Bargalló, N., Sánchez-Valle, R., Lladó, A., 2019. Clinical applicability of diagnostic biomarkers in early-onset cognitive impairment. Eur. J. Neurol. 26 (8), 1098–1104. https://doi.org/10.1111/ene.13945.

Fan, Z., Brooks, D.J., Okello, A., Edison, P., 2017. An early and late peak in microglial activation in Alzheimer's disease trajectory. Brain 140, 792–803. https://doi.org/10.1093/brain/aww349.

Feczko, E., Augustinack, J.C., Fischl, B., Dickerson, B.C., 2009. An MRI-based method for measuring volume, thickness and surface area of entorhinal, perirhinal, and posterior parahippocampal cortex. Neurobiol. Aging 30 (3), 420–431. https://doi.org/10.1016/j.neurobiolaging.2007.07.023.

Femminella, G.D., Ninan, S., Atkinson, R., Fan, Z., Brooks, D.J., Edison, P., 2016. Does Microglial Activation Influence Hippocampal Volume and Neuronal Function in Alzheimer's Disease and Parkinson's Disease Dementia? JAD 51 (4), 1275–1289. https://doi.org/10.3233/JAD-150827.

Fiford, C.M., Ridgway, G.R., Cash, D.M., Modat, M., Nicholas, J., Manning, E.N., Malone, I.B., Biessels, G.J., Ourselin, S., Carmichael, O.T., Cardoso, M.J., Barnes, J., 2018. Patterns of progressive atrophy vary with age in Alzheimer's disease patients. Neurobiol. Aging 63, 22–32. https://doi.org/10.1016/j.neurobiolaging.2017.11.002.

Fjell, A.M., Walhovd, K.B., Fennema-Notestine, C., McEvoy, L.K., Hagler, D.J., Holland, D., Brewer, J.B., Dale, A.M., 2010. CSF Biomarkers in Prediction of Cerebral and Clinical Change in Mild Cognitive Impairment and Alzheimer's Disease. J. Neurosci. 30 (6), 2088–2101. https://doi.org/10.1523/JNEUROSCI.3785-09.2010.

Fortea, J., Sala-Llonch, R., Bartrés-Faz, D., Lladó, A., Solé-Padullés, C., Bosch, B., Antonell, A., Olives, J., Sanchez-Valle, R., Molinuevo, J.L., Rami, L., 2011. Cognitively Preserved Subjects with Transitional Cerebrospinal Fluid ß-Amyloid 1-42 Values Have Thicker Cortex in Alzheimer's Disease Vulnerable Areas. Biol. Psychiatry 70 (2), 183–190. https://doi.org/10.1016/j.biopsych.2011.02.017.

Hamelin, L., Bertoux, M., Bottlaender, M., Corne, H., Lagarde, J., Hahn, V., Mangin, J.-F., Dubois, B., Chupin, M., de Souza, L.C., Colliot, O., Sarazin, M., 2015. Sulcal morphology as a new imaging marker for the diagnosis of early onset Alzheimer's disease. Neurobiol. Aging 36 (11), 2932–2939. https://doi.org/10.1016/j.neurobiolaging.2015.04.019.

Harper, L., Bouwman, F., Burton, E.J., Barkhof, F., Scheltens, P., O'Brien, J.T., Fox, N.C., Ridgway, G.R., Schott, J.M., 2017. Patterns of atrophy in pathologically confirmed dementias: a voxelwise analysis. J. Neurol. Neurosurg. Psychiatry 88 (11), 908–916. https://doi.org/10.1136/jnnp-2016-314978.

Hyman, B.T., Phelps, C.H., Beach, T.G., Bigio, E.H., Cairns, N.J., Carrillo, M.C., Dickson, D.W., Duyckaerts, C., Frosch, M.P., Masliah, E., Mirra, S.S., Nelson, P.T., Schneider, J.A., Thal, D.R., Thies, B., Trojanowski, J.Q., Vinters, H.V., Montine, T.J., 2012. National Institute on Aging-Alzheimer's Association guidelines for the neuropathologic assessment of Alzheimer's disease. Alzheimer's & Dementia 8 (1), 1–13. https://doi.org/10.1016/j.jalz.2011.10.007.

Insel, P.S., Mattsson, N., Mackin, R.S., Schöll, M., Nosheny, R.L., Tosun, D., Donohue, M. C., Aisen, P.S., Jagust, W.J., Weiner, M.W., 2016. Accelerating rates of cognitive decline and imaging markers associated with β-amyloid pathology. Neurology 86 (20), 1887–1896. https://doi.org/10.1212/WNL.0000000000002683.

Jack Jr., C.R., Bennett, D.A., Blennow, K., Carrillo, M.C., Dunn, B., Haeberlein, S.B., Holtzman, D.M., Jagust, W., Jessen, F., Karlawish, J., Liu, E., Molinuevo, J.L., Montine, T., Phelps, C., Rankin, K.P., Rowe, C.C., Scheltens, P., Siemers, E., Snyder, H.M., Sperling, R., Elliott, C., Masliah, E., Ryan, L., Silverberg, N., 2018. NIA-AA Research Framework: Toward a biological definition of Alzheimer's disease. Alzheimer's & Dementia 14 (4), 535–562. https://doi.org/10.1016/j.jalz.2018.02.018.

Jack, C.R., Bernstein, M.A., Fox, N.C., Thompson, P., Alexander, G., Harvey, D., Borowski, B., Britson, P.J., L. Whitwell, J., Ward, C., Dale, A.M., Felmlee, J.P., Gunter, J.L., Hill, D.L.G., Killiany, R., Schuff, N., Fox-Bosetti, S., Lin, C.,

Studholme, C., DeCarli, C.S., Gunnar Krueger, Ward, H.A., Metzger, G.J., Scott, K.T., Mallozzi, R., Blezek, D., Levy, J., Debbins, J.P., Fleisher, A.S., Albert, M., Green, R., Bartzokis, G., Glover, G., Mugler, J., Weiner, M.W., 2008. The Alzheimer's disease neuroimaging initiative (ADNI): MRI methods. J. Magn. Reson. Imaging 27 (4), 685–691. https://doi.org/10.1002/jmri.21049.

La Joie, R., Visani, A.V., Baker, S.L., Brown, J.A., Bourakova, V., Cha, J., Chaudhary, K., Edwards, L., Iaccarino, L., Janabi, M., Lesman-Segev, O.H., Miller, Z.A., Perry, D.C., O'Neil, J.P., Pham, J., Rojas, J.C., Rosen, H.J., Seeley, W.W., Tsai, R.M., Miller, B.L., Jagust, W.J., Rabinovici, G.D., 2020. Prospective longitudinal atrophy in Alzheimer's disease correlates with the intensity and topography of baseline tau-PET. Sci. Transl. Med. 12 (524), eaau5732. https://doi.org/10.1126/scitranslmed.aau5732.

Kaur, G., Poljak, A., Braidy, N., Crawford, J.D., Lo, J., Sachdev, P.S., 2020. Fluid Biomarkers and APOE Status of Early Onset Alzheimer's Disease Variants: A Systematic Review and Meta-Analysis. JAD 75 (3), 827–843. https://doi.org/10.3233/JAD-200052.

Koedam, E.L.G.E., Lauffer, V., van der Vlies, A.E., van der Flier, W.M., Scheltens, P., Pijnenburg, Y.A.L., 2010. Early-Versus Late-Onset Alzheimer's Disease: More than Age Alone. JAD 19 (4), 1401–1408. https://doi.org/10.3233/JAD-2010-1337.

Kreisl, W.C., Lyoo, C.H., McGwier, M., Snow, J., Jenko, K.J., Kimura, N., Corona, W., Morse, C.L., Zoghbi, S.S., Pike, V.W., McMahon, F.J., Turner, R.S., Innis, R.B., 2013. In vivo radioligand binding to translocator protein correlates with severity of Alzheimer's disease. Brain 136, 2228–2238. https://doi.org/10.1093/brain/awt145.

Landau, S.M., Breault, C., Joshi, A.D., Pontecorvo, M., Mathis, C.A., Jagust, W.J., Mintun, M.A., 2013. Amyloid-β Imaging with Pittsburgh Compound B and Florbetapir: Comparing Radiotracers and Quantification Methods and Initiative for the Alzheimer's Disease Neuroimaging. Soc. Nucl. Med. 54, 70–77. https://doi.org/10.2967/jnumed.112.109009.Amyloid-.

Lee, E.C., Kang, J.M., Seo, S., Seo, H.E., Lee, S.Y., Park, K.H., Na, D.L., Noh, Y., Seong, J.K., 2020. Association of Subcortical Structural Shapes With Tau, Amyloid, and Cortical Atrophy in Early-Onset and Late-Onset Alzheimer's Disease. Front. Aging Neurosci. 12, 1–11. https://doi.org/10.3389/fnagi.2020.563559.

Marshall, G.A., Fairbanks, L.A., Tekin, S., Vinters, H.V., Cummings, J.L., 2007. Early-Onset Alzheimer's Disease Is Associated With Greater Pathologic Burden. J. Geriatr. Psychiatry Neurol. 20 (1), 29–33. https://doi.org/10.1177/0891988706297086.

Mattsson, N., Ossenkoppele, R., Smith, R., Strandberg, O., Ohlsson, T., Jögi, J., Palmqvist, S., Stomrud, E., Hansson, O., 2018. Greater tau load and reduced cortical thickness in APOE ε4-negative Alzheimer's disease: a cohort study. Alzheimer's Res. Ther. 10, 1–12. https://doi.org/10.1186/s13195-018-0403-x.

McKhann, G.M., Knopman, D.S., Chertkow, H., Hyman, B.T., Jack Jr., C.R., Kawas, C.H., Klunk, W.E., Koroshetz, W.J., Manly, J.J., Mayeux, R., Mohs, R.C., Morris, J.C., Rossor, M.N., Scheltens, P., Carrillo, M.C., Thies, B., Weintraub, S., Phelps, C.H., 2011. The diagnosis of dementia due to Alzheimer's disease: Recommendations from the National Institute on Aging-Alzheimer's Association workgroups on diagnostic guidelines for Alzheimer's disease. Alzheimer's & Dementia 7 (3), 263–269. https://doi.org/10.1016/j.jalz.2011.03.005.

Mendez, M.F., 2012. Early-onset Alzheimer's Disease: Nonamnestic Subtypes and Type 2 AD. Arch. Med. Res. 43 (8), 677–685. https://doi.org/10.1016/j.arcmed.2012.11.009.

Migliaccio, R., Agosta, F., Possin, K.L., Canu, E., Filippi, M., Rabinovici, G.D., Rosen, H.J., Miller, B.L., Gorno-Tempini, M.L., Galimberti, D., 2015. Mapping the Progression of Atrophy in Early- and Late-Onset Alzheimer's Disease. JAD 46 (2), 351–364. https://doi.org/10.3233/JAD-142292.

Möller, C., Vrenken, H., Jiskoot, L., Versteeg, A., Barkhof, F., Scheltens, P., van der Flier, W.M., 2013. Different patterns of gray matter atrophy in early- and late-onset Alzheimer's disease. Neurobiol. Aging 34 (8), 2014–2022. https://doi.org/10.1016/j.neurobiolaging.2013.02.013.

Murray, M.E., Graff-Radford, N.R., Ross, O.A., Petersen, R.C., Duara, R., Dickson, D.W., 2011. Neuropathologically defined subtypes of Alzheimer's disease with distinct clinical characteristics: a retrospective study. Lancet Neurology 10 (9), 785–796. https://doi.org/10.1016/S1474-4422(11)70156-9.

Ossenkoppele, R., Cohn-Sheehy, B.I., La Joie, R., Vogel, J.W., Möller, C., Lehmann, M., van Berckel, B.N.M., Seeley, W.W., Pijnenburg, Y.A., Gorno-Tempini, M.L., Kramer, J.H., Barkhof, F., Rosen, H.J., van der Flier, W.M., Jagust, W.J., Miller, B.L., Scheltens, P., Rabinovici, G.D., 2015a. Atrophy patterns in early clinical stages across distinct phenotypes of Alzheimer's disease: Origin and Spread of Atrophy in AD Variants. Hum. Brain Mapp. 36 (11), 4421–4437. https://doi.org/10.1002/hbm.22927.

Ossenkoppele, R., Mattsson, N., Teunissen, C.E., Barkhof, F., Pijnenburg, Y., Scheltens, P., van der Flier, W.M., Rabinovici, G.D., 2015b. Cerebrospinal fluid biomarkers and cerebral atrophy in distinct clinical variants of probable Alzheimer's disease. Neurobiol. Aging 36 (8), 2340–2347. https://doi.org/10.1016/j.neurobiolaging.2015.04.011.

Ossenkoppele, R., Zwan, M.D., Tolboom, N., van Assema, D.M.E., Adriaanse, S.F., Kloet, R.W., Boellaard, R., Windhorst, A.D., Barkhof, F., Lammertsma, A.A., Scheltens, P., van der Flier, W.M., van Berckel, B.N.M., 2012. Amyloid burden and

metabolic function in early-onset Alzheimer's disease: parietal lobe involvement. Brain 135 (7), 2115–2125. https://doi.org/10.1093/brain/aws113.

Palmqvist, S., Schöll, M., Strandberg, O., Mattsson, N., Stomrud, E., Zetterberg, H., Blennow, K., Landau, S., Jagust, W., Hansson, O., 2017. Earliest accumulation of β-amyloid occurs within the default-mode network and concurrently affects brain connectivity. Nat Commun 8 (1). https://doi.org/10.1038/s41467-017-01150-x.

Parbo, P., Ismail, R., Sommerauer, M., Stokholm, M.G., Hansen, A.K., Hansen, K.V., Amidi, A., Schaldemose, J.L., Gottrup, H., Brændgaard, H., Eskildsen, S.F., Borghammer, P., Hinz, R., Aanerud, J., Brooks, D.J., 2018. Does inflammation precede tau aggregation in early Alzheimer's disease? A PET study. Neurobiol. Disease 117, 211–216. https://doi.org/10.1016/j.nbd.2018.06.004.

Peguereles, J., Vilaplana, E., Montal, V., Sampedro, F., Alcolea, D., Carmona-Iragui, M., Clarimon, J., Blesa, R., Lleó, A., Fortea, J., 2017. Longitudinal brain structural changes in preclinical Alzheimer's disease. Alzheimer's & Dementia 13 (5), 499–509. https://doi.org/10.1016/j.jalz.2016.08.010.

Pillai, J.A., Larvie, M., Chen, J., Crawford, A., Cummings, J.L., Jones, S.E., 2020. Spatial patterns of correlation between cortical amyloid and cortical thickness in a tertiary clinical population with memory deficit. Sci. Rep. 10, 1–13. https://doi.org/10.1038/s41598-020-77503-2.

Reuter, M., Schmansky, N.J., Rosas, H.D., Fischl, B., 2012. Within-subject template estimation for unbiased longitudinal image analysis. NeuroImage 61 (4), 1402–1418. https://doi.org/10.1016/j.neuroimage.2012.02.084.

Risacher, S.L., Shen, L.i., West, J.D., Kim, S., McDonald, B.C., Beckett, L.A., Harvey, D.J., Jack Jr., C.R., Weiner, M.W., Saykin, A.J., 2010. Longitudinal MRI atrophy biomarkers: Relationship to conversion in the ADNI cohort. Neurobiol. Aging 31 (8), 1401–1418. https://doi.org/10.1016/j.neurobiolaging.2010.04.029.

Savva, G.M., Wharton, S.B., Ince, P.G., Forster, G., Matthews, F.E., Brayne, C., 2009. Age, Neuropathology, and Dementia. N Engl J Med 360 (22), 2302–2309. https://doi.org/10.1056/NEJMoa0806142.

Schöll, M., Ossenkoppele, R., Strandberg, O., Palmqvist, S., Jögi, J., Ohlsson, T., Smith, R., Hansson, O., 2017. Distinct 18F-AV-1451 tau PET retention patterns in early- and late-onset Alzheimer's disease. Brain 140, 2286–2294. https://doi.org/10.1093/brain/awx171.

Seidman, L.J., Faraone, S.V., Goldstein, J.M., Goodman, J.M., Kremen, W.S., Matsuda, G., Hoge, E.A., Kennedy, D., Makris, N., Caviness, V.S., Tsuang, M.T., 1997. Reduced subcortical brain volumes in nonpsychotic siblings of schizophrenic patients: A pilot magnetic resonance imaging study. Am. J. Med. Genet. - Neuropsychiatr. Genet. 74, 507–514. https://doi.org/10.1002/(SICI)1096-8628(19970919)74:5<507::AID-AJMG11>3.0.CO;2-G.

Shaw, L.M., Vanderstichele, H., Knapik-Czajka, M., Clark, C.M., Aisen, P.S., Petersen, R.C., Blennow, K., Soares, H., Simon, A., Lewczuk, P., Dean, R., Siemers, E., Potter, W., Lee, V.-Y., Trojanowski, J.Q., 2009. Cerebrospinal fluid biomarker signature in Alzheimer's disease neuroimaging initiative subjects. Ann Neurol. 65 (4), 403–413. https://doi.org/10.1002/ana.21610.

Tarawneh, R., Head, D., Allison, S., Buckles, V., Fagan, A.M., Ladenson, J.H., Morris, J.C., Holtzman, D.M., 2015. Cerebrospinal Fluid Markers of Neurodegeneration and Rates of Brain Atrophy in Early Alzheimer Disease. JAMA Neurol. 72 (6), 656. https://doi.org/10.1001/jamaneurol.2015.0202.

Thijssen, E.H., La Joie, R., Wolf, A., Strom, A., Wang, P., Iaccarino, L., Bourakova, V., Cobigo, Y., Heuer, H., Spina, S., VandeVrede, L., Chai, X., Proctor, N.K., Airey, D.C., Shcherbinin, S., Duggan Evans, C., Sims, J.R., Zetterberg, H., Blennow, K., Karydas, A.M., Teunissen, C.E., Kramer, J.H., Grinberg, L.T., Seeley, W.W., Rosen, H., Boeve, B.F., Miller, B.L., Rabinovici, G.D., Dage, J.L., Rojas, J.C., Boxer, A.L., 2020. Diagnostic value of plasma phosphorylated tau181 in Alzheimer's disease and frontotemporal lobar degeneration. Nat. Med. 26 (3), 387–397. https://doi.org/10.1038/s41591-020-0762-2.

van de Pol, L.A., Hensel, A., Barkhof, F., Gertz, H.J., Scheltens, P., van der Flier, W.M., 2006. Hippocampal atrophy in Alzheimer disease: Age matters. Neurology 66 (2), 236–238. https://doi.org/10.1212/01.wnl.0000194240.47892.4d.

Wattmo, C., Wallin, Å.K., 2017. Early- versus late-onset Alzheimer's disease in clinical practice: cognitive and global outcomes over 3 years. Alzheimers. Res. Ther. 9, 70. https://doi.org/10.1186/s13195-017-0294-2.

Whitwell, J.L., Dickson, D.W., Murray, M.E., Weigand, S.D., Tosakulwong, N., Senjem, M.L., Knopman, D.S., Boeve, B.F., Parisi, J.E., Petersen, R.C., Jack Jr, C.R., Josephs, K.A., 2012. Neuroimaging correlates of pathologically defined subtypes of Alzheimer's disease: a case-control study. Lancet Neurology 11 (10), 868–877. https://doi.org/10.1016/S1474-4422(12)70200-4.

Whitwell, J.L., Graff-Radford, J., Tosakulwong, N., Weigand, S.D., Machulda, M.M., Senjem, M.L., Spychalla, A.J., Vemuri, P., Jones, D.T., Drubach, D.A., Knopman, D.S., Boeve, B.F., Ertekin-Taner, N., Petersen, R.C., Lowe, V.J., Jack Jr., C.R., Josephs, K.A., 2018. Imaging correlations of tau, amyloid, metabolism, and atrophy in typical and atypical Alzheimer's disease. Alzheimer's & Dementia 14 (8), 1005–1014. https://doi.org/10.1016/j.jalz.2018.02.020.

Zetterberg, H., Skillbäck, T., Mattsson, N., Trojanowski, J.Q., Portelius, E., Shaw, L.M., Weiner, M.W., Blennow, K., 2016. Association of Cerebrospinal Fluid Neurofilament Light Concentration With Alzheimer Disease Progression. JAMA Neurol 73 (1), 60. https://doi.org/10.1001/jamaneurol.2015.3037.